SCIENTIFIC REPORTS
nature research

OPEN

TAO-DFT investigation of electronic properties of linear and cyclic carbon chains

Sonai Seenithurai[1] & Jeng-Da Chai[1,2]✉

It has been challenging to adequately investigate the properties of nanosystems with radical nature using conventional electronic structure methods. We address this challenge by calculating the electronic properties of linear carbon chains (*l*-CC[*n*]) and cyclic carbon chains (*c*-CC[*n*]) with *n* = 10–100 carbon atoms, using thermally-assisted-occupation density functional theory (TAO-DFT). For all the cases investigated, *l*-CC[*n*]/*c*-CC[*n*] are ground-state singlets, and *c*-CC[*n*] are energetically more stable than *l*-CC[*n*]. The electronic properties of *l*-CC[*n*]/*c*-CC[*n*] reveal certain oscillation patterns for smaller *n*, followed by monotonic changes for larger *n*. For the smaller carbon chains, odd-numbered *l*-CC[*n*] are more stable than the adjacent even-numbered ones; *c*-CC[4*m* + 2]/*c*-CC[4*m*] are more/less stable than the adjacent odd-numbered ones, where *m* are positive integers. As *n* increases, *l*-CC[*n*]/*c*-CC[*n*] possess increasing polyradical nature in their ground states, where the active orbitals are delocalized over the entire length of *l*-CC[*n*] or the whole circumference of *c*-CC[*n*].

Carbon is the most versatile element in forming various structures. In bulk phase, graphite and diamond, which are well-known materials, have been used for centuries. In nanoforms, fullerenes and graphene have been studied in detail for decades. In general, nanostructures can be classified into three categories: zero-dimensional (0D), one-dimensional (1D), and two-dimensional (2D) nanomaterials. Carbon forms all these nanostructures with unique shapes and properties. Over the past few decades, carbon nanomaterials have been widely studied, and applied in diverse industries[1–3].

A number of carbon nanostructures have been synthesized and applied in different fields. The 0D carbon nanomaterials include clusters, quantum dots, nanoflakes, and buckyballs[3]. Among them, the C_{60} fullerene molecule (containing 12 pentagons and 20 hexagons), where the carbon atoms are sp^2–sp^3-hybridized, has been a popular carbon nanomaterial[1]. The discovery of C_{60} has led to the flourishment of carbon nanomaterials in various ways.

Graphite is a bulk layered material, where the sp^2-hybridized carbon atoms in each layer are arranged in a hexagonal lattice. The 2D carbon nanomaterial, graphene, can be obtained by mechanically exfoliating a single layer of carbon atoms from graphite[2]. Thus, graphene, which is a perfect arrangement of hexagons made up of sp^2-hybridized carbon atoms in a 2D planar surface, can be the thinnest (i.e., single-atom-thick) material synthesized ever. Graphene is a zero-gap semiconductor or semimetal with massless Dirac fermions with linear dispersion at low energy. Because of the Dirac-cone feature, graphene has huge potential in electronics applications[2]. The discovery of graphene has also led to the discovery of other 2D materials. Besides, if a graphene sheet can be rolled up to form a seamless cylinder, one obtains a carbon nanotube (CNT), which belongs to the class of 1D nanostructures. Note that CNTs were first observed by Iijima in 1991[4], well before the separation and characterization of graphene. On the basis of the direction of rolling (chirality), CNTs can be classified into three groups: chiral, zigzag, and armchair CNTs, which can have rather different electronic properties.

Apart from these well studied carbon nanoallotropes, linear carbon chains (i.e., also belonging to the class of 1D nanostructures), where the carbon atoms are *sp*-hybridized, have recently gained much attention because of their interesting physical and chemical properties[5–18]. A linear carbon chain consisting of *n* carbon atoms (for brevity, denoted as *l*-CC[*n*] (see Fig. 1a)) is an ideal 1D carbon nanomaterial. Kroto et al. originally designed an experiment for explaining the formation mechanism of carbon chains in outer space, which led to

[1]Department of Physics, National Taiwan University, Taipei 10617, Taiwan. [2]Center for Theoretical Physics and Center for Quantum Science and Engineering, National Taiwan University, Taipei 10617, Taiwan. ✉email: jdchai@phys.ntu.edu.tw

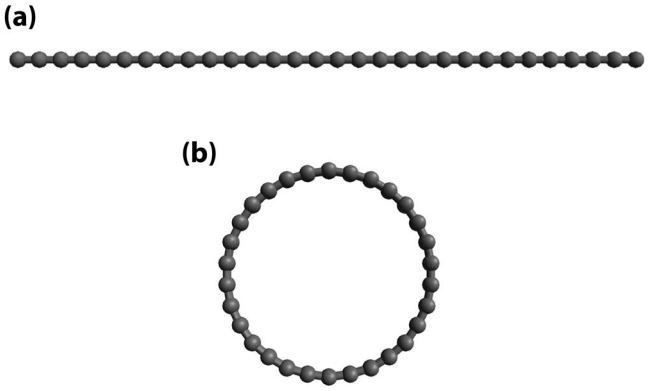

Figure 1. Structures of (**a**) *l*-CC[30] and (**b**) *c*-CC[30], each consisting of 30 carbon atoms.

the serendipitous discovery of C_{60}[1]. In attempting to synthesize *l*-CC[*n*] (i.e., the holy grail of truly 1D carbon allotropes), significant progresses have been made recently[6,11,14]. Owing to their high reactivity, pristine linear carbon chains have not yet been reported. However, the linear carbon chains (containing up to 100 carbon atoms) supported inside multi-walled CNTs were realized in 2003 by Zhao et al.[6]. In 2015, Andrade et al.[11] observed the carbon chains inside CNTs under high pressures. In 2016, Shi et al.[14] demonstrated the large-scale syntheses of linear carbon chains inside double-walled CNTs by using the confined space inside the tube as a nanoreactor to grow ultra-long carbon chains (containing up to 6400 carbon atoms) in large quantities[14,15]. Linear carbon chains can be potential candidates for nanodevices, molecular electronics, and the building blocks of novel hybrid nanomaterials (e.g., sp–sp^2 and sp–sp^3 hybridized materials) by integrating with other nanostructures[8,9,17]. On the theoretical side, a number of relevant calculations are available[9]. The calculations showed that the linear carbon chains inside single-walled CNTs can modify the electronic properties of pristine single-walled CNTs significantly. It has been found that the chirality of the enclosing nanotubes can affect the properties of linear carbon chains[18]. Besides, recent theoretical studies showed that linear carbon chains have excellent mechanical and electrical properties[9,10,14].

On the other hand, cyclic carbon chains (for brevity, denoted as *c*-CC[*n*] (see Fig. 1b)), which are the monocyclic isomers of linear carbon chains, have also attracted considerable attention in recent years[19–38]. Note that *c*-CC[*n*] (where the carbon atoms are also sp-hybridized) are hypothesized to be the building blocks of fullerenes in the initial stages of growth[21]. Interestingly, *c*-CC[$4m + 2$] (where m are positive integers) have been found to possess high stability[24,25]. Among them, *c*-CC[18] has recently been synthesized[26], and some of the electronic properties of *c*-CC[18] have been reported. There are also a few theoretical studies on the electronic properties and applications of *c*-CC[18] and other cyclic carbon chains[22,27–38]. For example, *c*-CC[18] has been found to possess electron-acceptor properties, and can be dubbed as the smallest all-carbon electron acceptor[28].

In general, it remains extremely difficult to synthesize both *l*-CC[*n*] and *c*-CC[*n*]. Accordingly, theoretical studies are complementary, and may provide immense information on the properties of *l*-CC[*n*] and *c*-CC[*n*]. In a recent theoretical study, it has been reported that very small *l*-CC[*n*] (n = 5–10) with even n values possess diradical nature in their ground states[16]. Therefore, it can be anticipated that the larger *l*-CC[*n*] and *c*-CC[*n*] could also possess radical character due to the low dimensionality of *l*-CC[*n*] and *c*-CC[*n*], respectively[39]. Despite its success in describing some ground-state properties, Kohn-Sham density functional theory (KS-DFT)[40] can yield unreliable results for systems with radical nature[41], when the conventional XC density functionals are employed. Typically, multi-reference (MR) electronic structure methods, such as the complete-active-space self-consistent-field (CASSCF), complete-active-space second-order perturbation theory (CASPT2), and related methods[42–48], are required to reliably predict the energy and related properties of systems with radical nature. Nonetheless, accurate MR electronic structure methods can be prohibitively expensive for large systems, and hence may not be practical for studying the properties of the larger *l*-CC[*n*] and *c*-CC[*n*].

Recently, thermally-assisted-occupation density functional theory (TAO-DFT)[49], which is a density functional theory with fractional orbital occupation numbers, has been formulated to tackle such challenging problems (i.e., nanosystems with radical nature), wherein an entropy contribution term (i.e., a function of the fictitious temperature θ and orbital occupation numbers) can approximately describe strong static correlation even when the simplest local density approximation (LDA) XC density functional is employed. In TAO-DFT, one can also adopt more sophisticated XC density functionals, such as semilocal[50], global hybrid[51], and range-separated hybrid[51,52] XC density functionals. Besides, aiming to improve the accuracy of TAO-DFT for a wide range of applications, a self-consistent scheme determining the fictitious temperature θ in TAO-DFT has been recently proposed[53]. Since TAO-DFT is a computationally efficient electronic structure method, a number of strongly correlated electron systems at the nanoscale have been studied using TAO-DFT in recent years[16,54–62]. Besides, TAO-DFT has been recently shown to be useful in describing the vibrational spectra of molecules with radical nature[63]. In addition, TAO-DFT and related methods have recently been employed to investigate the electronic properties of several nanosystems with radical nature[64,65], and have also been combined with the linear-scaling divide-and-conquer approach for the study of large systems with strong static correlation effects[66].

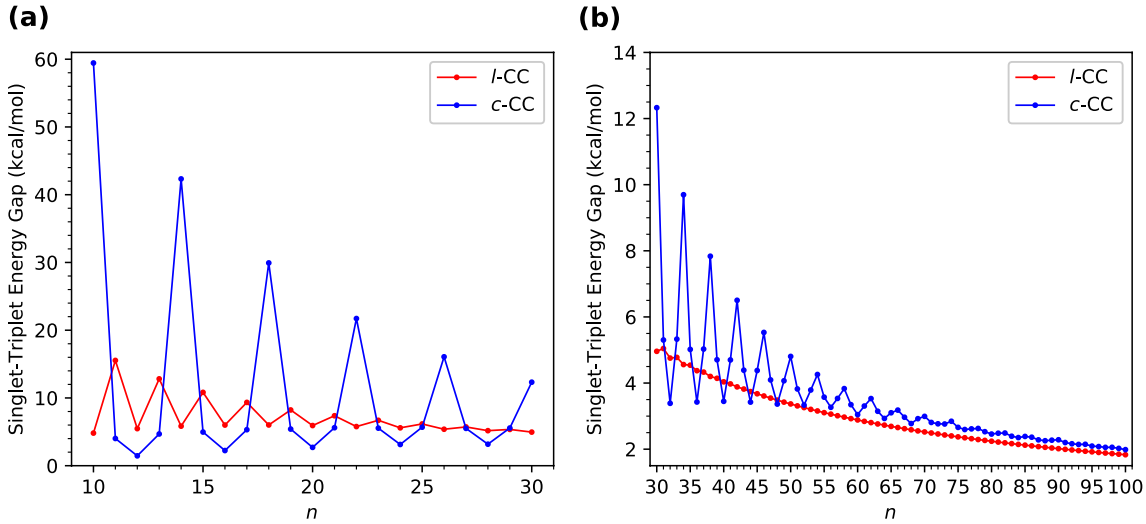

Figure 2. Singlet-triplet energy gap of l-CC[n]/c-CC[n] with (**a**) n = 10–30 and (**b**) n = 30–100, calculated using spin-unrestricted TAO-LDA.

Therefore, in the present study, we carry out TAO-DFT calculations to investigate the electronic properties of l-CC[n]/c-CC[n] with n = 10–100. Specifically, we report the electronic properties, such as the singlet-triplet energy gap, singlet-quintet energy gap, vertical ionization potential, vertical electron affinity, fundamental gap, symmetrized von Neumann entropy, active orbital occupation numbers, real-space representation of active orbitals, and relative stability of l-CC[n]/c-CC[n]. For considerably large values of n, we show that both l-CC[n] and c-CC[n] are polyradicals in their ground states, playing an important role in determining their electronic properties.

Computational details

All geometry optimizations and other calculations are performed with Q-Chem 4.4[67], using the 6-31G(d) basis set (i.e., a valence double-zeta polarized basis set) with a numerical quadrature that consists of 75 points in the Euler-Maclaurin radial grid and 302 points in the Lebedev angular grid. We carry out calculations using TAO-LDA[49], which is TAO-DFT employing the LDA XC and θ-dependent density functionals, with the recommended fictitious temperature θ = 7 mhartree[49].

In several recent studies[46,48,49,54,55], the orbital occupation numbers obtained from TAO-LDA (with θ = 7 mhartree) have been found to be qualitatively similar to the natural orbital occupation numbers obtained from the variational two-electron reduced-density-matrix-driven CASSCF (v2RDM-CASSCF) method (i.e., an accurate MR electronic structure method), leading to a similar trend for the radical nature of several systems.

Results and discussion

Singlet-triplet energy gap and singlet-quintet energy gap. Aiming to obtain the energetically preferred spin state (i.e., the ground state) of l-CC[n]/c-CC[n], we obtain the energies of l-CC[n]/c-CC[n] for the lowest singlet, triplet, and quintet states by optimizing the corresponding structures with spin-unrestricted TAO-LDA, and thereafter compute the singlet-triplet energy gap of l-CC[n]/c-CC[n] using

$$E_{ST} = E_T - E_S, \tag{1}$$

and compute the singlet-quintet energy gap of l-CC[n]/c-CC[n] using

$$E_{SQ} = E_Q - E_S, \tag{2}$$

where E_Q, E_T, and E_S are the lowest quintet, triplet, and singlet energies, respectively, of l-CC[n]/c-CC[n] (also see Section I, Figure S1, and Figure S2 in Supplementary Information (SI)). According to their definitions, the E_{ST} and E_{SQ} reported in this work are the adiabatic singlet-triplet energy gap and adiabatic singlet-quintet energy gap, respectively, of l-CC[n]/c-CC[n]. The E_{ST} and E_{SQ} values of l-CC[n]/c-CC[n] as functions of the number of carbon atoms are presented in Figs. 2 and 3, respectively (also see Tables S1 and S2 in SI).

Since the E_{ST} and E_{SQ} values remain positive, the l-CC[n]/c-CC[n] studied are all ground-state singlets. The E_{ST} values of the smaller l-CC[n] exhibit an odd-even oscillation pattern in which the E_{ST} values of odd-numbered l-CC[n] are larger than those of the adjacent even-numbered ones. However, such oscillations decrease with increasing n, and eventually disappear for considerably large n. Accordingly, the E_{ST} values of l-CC[n] are oscillatory only for smaller values of n (up to n = 33), and become monotonically decreasing for larger n. The E_{SQ} values of l-CC[n] decrease essentially monotonically with n (i.e., except only for n = 10).

By contrast, the E_{ST} and E_{SQ} values of the smaller c-CC[n] display distinct oscillation patterns in which the E_{ST} and E_{SQ} values of c-CC[$4m + 2$]/c-CC[$4m$] are larger/smaller than the E_{ST} and E_{SQ} values, respectively, of the adjacent odd-numbered ones, where m are positive integers. Nevertheless, with the increase of molecular size, these oscillations are progressively reduced, and eventually absent for sufficiently large n. Therefore, the

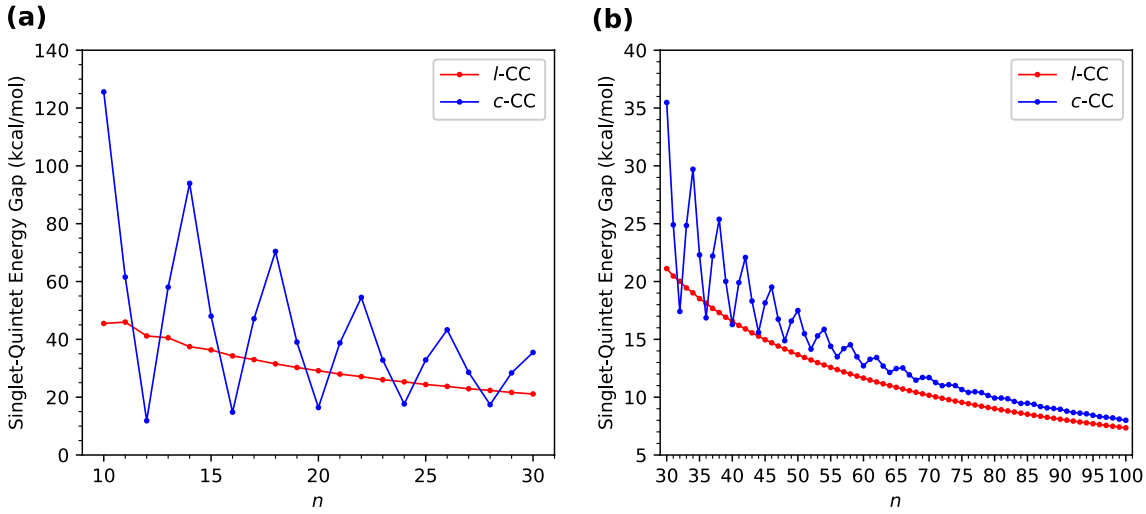

Figure 3. Singlet-quintet energy gap of *l*-CC[*n*]/*c*-CC[*n*] with (**a**) *n* = 10–30 and (**b**) *n* = 30–100, calculated using spin-unrestricted TAO-LDA.

E_{ST} and E_{SQ} values of *c*-CC[*n*] are oscillatory only for smaller *n* (up to *n* = 94 for E_{ST} and up to *n* = 85 for E_{SQ}), and become monotonically decreasing for larger values of *n*. Note that the reasons for these oscillation patterns have been recently provided in a quantum Monte Carlo study[34].

Understanding the E_{ST} values is essential for applications that involve harnessing energy through the singlet-fission phenomenon[68]. Consequently, the E_{ST} values of *l*-CC[*n*]/*c*-CC[*n*] reported in the present study can provide insight into the singlet-fission phenomenon. For other relevant applications, it is worth mentioning that the electronic transport properties of *c*-CC[18]-based molecular devices have been recently studied[38].

Vertical ionization potential, vertical electron affinity, and fundamental gap. Here, we assess if *l*-CC[*n*]/*c*-CC[*n*] are promising for photovoltaic applications. For a molecule in its ground state, the vertical ionization potential (IP_v) is the energy required to remove an electron from the molecule without affecting the molecular geometry, the vertical electron affinity (EA_v) is the energy released when an electron is added to the molecule without affecting the molecular geometry, and the fundamental gap (E_g) is the difference between IP_v and EA_v (i.e., $E_g = IP_v - EA_v$). Accordingly, in this work, we calculate the vertical ionization potential of ground-state *l*-CC[*n*]/*c*-CC[*n*] using

$$IP_v = E_{N-1} - E_N, \tag{3}$$

the vertical electron affinity of ground-state *l*-CC[*n*]/*c*-CC[*n*] using

$$EA_v = E_N - E_{N+1}, \tag{4}$$

and the fundamental gap of ground-state *l*-CC[*n*]/*c*-CC[*n*] using

$$E_g = E_{N+1} + E_{N-1} - 2E_N, \tag{5}$$

where E_N is the total energy of the *N*-electron molecule (i.e., *l*-CC[*n*]/*c*-CC[*n*]) at the ground-state (i.e., lowest singlet state) geometry, obtained with spin-unrestricted TAO-LDA. The IP_v (Fig. 4a), EA_v (Fig. 4b), and E_g (Fig. 4c) values of ground-state *l*-CC[*n*]/*c*-CC[*n*] are plotted as functions of *n* (also see Tables S3 and S4 in SI).

As *n* increases, the IP_v value of *l*-CC[*n*] decreases monotonically, showing a very slight odd-even pattern only for very small *n*. The EA_v/E_g values of the smaller *l*-CC[*n*] reveal an odd-even oscillation pattern in which the EA_v/E_g values of odd-numbered *l*-CC[*n*] are smaller/larger than those of the adjacent even-numbered ones. Nevertheless, with the increase of *n*, these oscillations are progressively reduced, and ultimately absent for sufficiently large *n*. Accordingly, the EA_v/E_g values of *l*-CC[*n*] are oscillatory only for smaller *n* (up to *n* = 21 for EA_v and up to *n* = 15 for E_g), and become monotonically increasing/decreasing for larger values of *n*.

On the other hand, the $IP_v/EA_v/E_g$ values of the smaller *c*-CC[*n*] display a distinct oscillation pattern in which the $IP_v/EA_v/E_g$ values of *c*-CC[$4m + 2$] are larger/smaller/larger than those of the adjacent odd-numbered ones, where *m* are positive integers. Nonetheless, such oscillations are gradually reduced, and eventually absent with the increase of molecular size. Therefore, the $IP_v/EA_v/E_g$ values of *c*-CC[*n*] are oscillatory only for smaller values of *n* (up to *n* = 61 for IP_v, up to *n* = 58 for EA_v, and up to *n* = 46 for E_g), and become monotonically decreasing/increasing/decreasing for larger *n*.

For each *n*, the E_g value of *c*-CC[*n*] is larger than that of *l*-CC[*n*]. Besides, the E_g values of *l*-CC[*n*] (with *n* = 24–100) and *c*-CC[*n*] (with *n* = 31–100) are in the range of 1 to 3 eV, showing promise for their applications in nanophotonics.

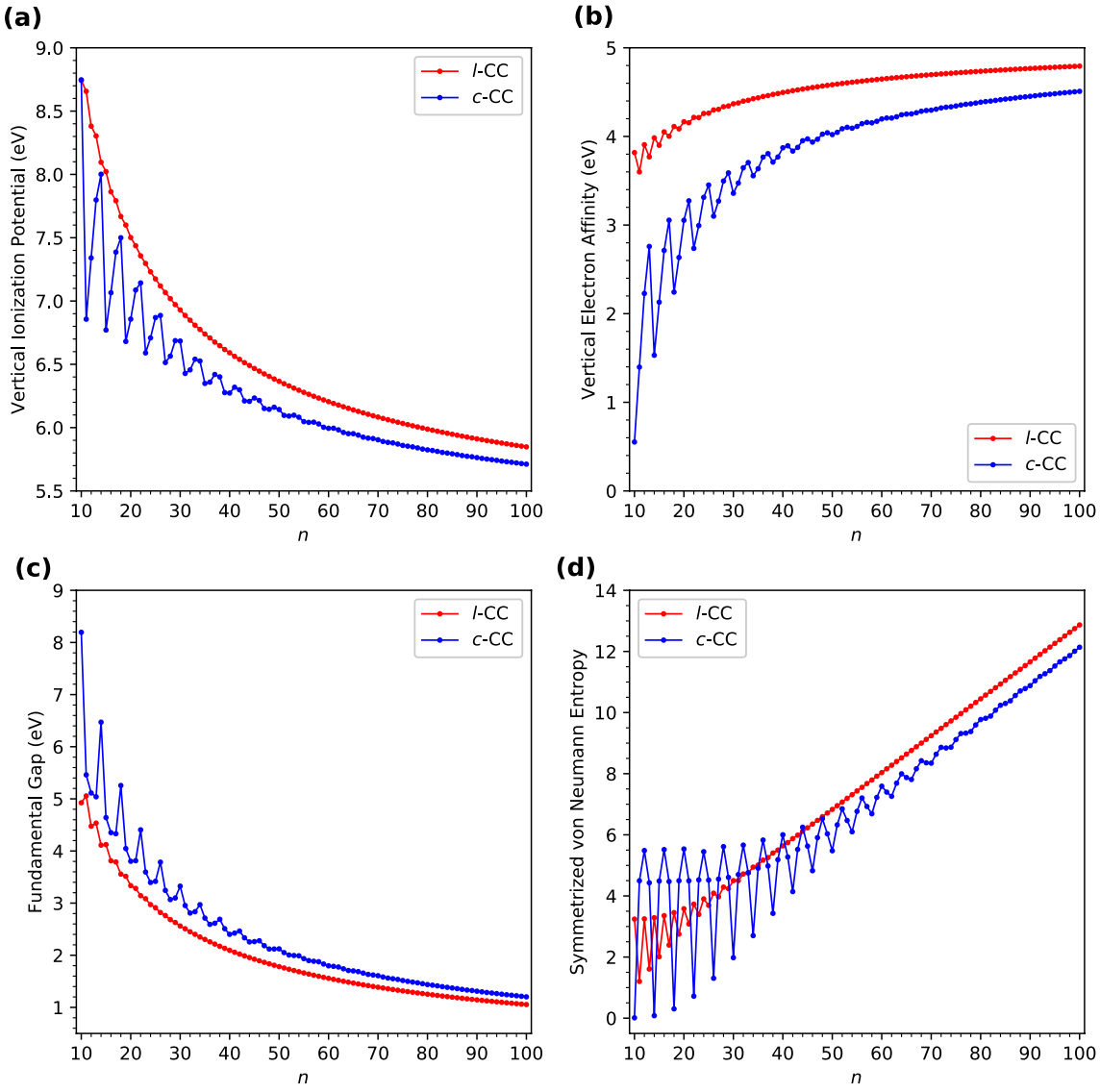

Figure 4. (**a**) Vertical ionization potential, (**b**) vertical electron affinity, (**c**) fundamental gap, and (**d**) symmetrized von Neumann entropy of ground-state l-CC[n]/c-CC[n] with n = 10–100, calculated using spin-unrestricted TAO-LDA.

Symmetrized von Neumann entropy. To assess the radical nature of ground-state (i.e., lowest singlet state) l-CC[n]/c-CC[n], we calculate the symmetrized von Neumann entropy[16,50,51,54,56–62,69]

$$S_{\mathrm{vN}} = -\frac{1}{2}\sum_{\sigma=\uparrow,\downarrow}\sum_{i=1}^{\infty}\left\{f_{i,\sigma}\,\ln(f_{i,\sigma}) + (1-f_{i,\sigma})\,\ln(1-f_{i,\sigma})\right\}, \tag{6}$$

using spin-unrestricted TAO-LDA. Here, the occupation number $f_{i,\sigma}$ of the ith σ-spin orbital (i.e., up-spin orbital or down-spin orbital) obtained with spin-unrestricted TAO-LDA, which ranges from 0 to 1, is closely related to the occupation number of the ith σ-spin natural orbital[49–51]. For a molecule with nonradical nature, the occupation numbers of all spin-orbitals should be close to either 0 or 1, leading to insignificant contributions to the corresponding S_{vN} value. However, for a molecule with pronounced radical nature, the occupation numbers of active spin-orbitals (i.e., the spin-orbitals that have considerable fractional occupations) can be very different from 0 and 1 (e.g., between 0.1 and 0.9); hence, the corresponding S_{vN} value is expected to increase when the occupation numbers of active spin-orbitals become closer to 0.5 and/or the number of active spin-orbitals increases.

As shown in Fig. 4d, the S_{vN} values of ground-state l-CC[n] and c-CC[n] possess rather different oscillation patterns (also see Tables S3 and S4 in SI). The S_{vN} values of the smaller l-CC[n] exhibit an odd-even oscillation pattern in which the S_{vN} values of odd-numbered l-CC[n] are smaller than those of the adjacent even-numbered ones. Nonetheless, when the system size increases, such oscillations are gradually damped, and ultimately absent for considerably large n. Therefore, the S_{vN} values of l-CC[n] are oscillatory only for smaller n (up to n = 29),

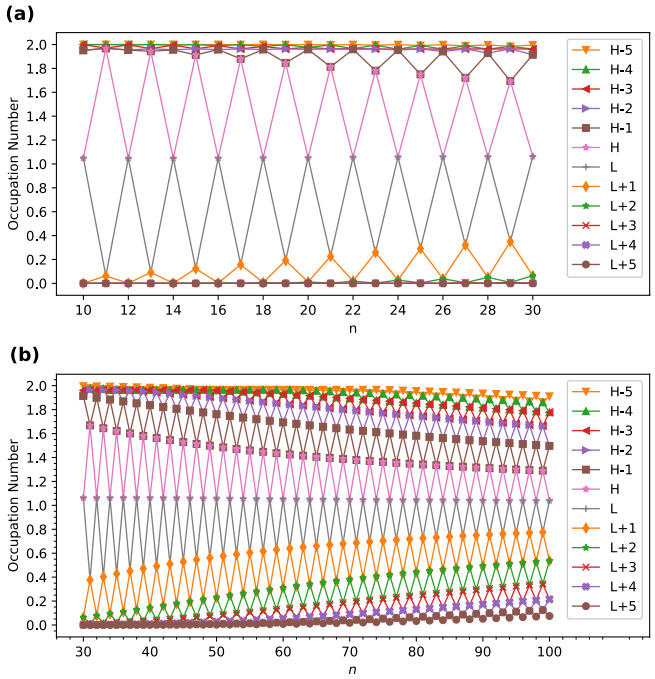

Figure 5. Active orbital occupation numbers (HOMO−5,...,HOMO−1, HOMO, LUMO, LUMO+1,...,and LUMO+5) of ground-state l-CC[n] with (**a**) n = 10–30 and (**b**) n = 30–100, calculated using spin-restricted TAO-LDA. For brevity, HOMO/LUMO is denoted as H/L.

and become monotonically increasing for larger n. By contrast, the S_{vN} values of the smaller c-CC[n] reveal a distinct oscillation pattern in which the S_{vN} values of c-CC[$4m + 2$]/c-CC[$4m$] are smaller/larger than those of the adjacent odd-numbered ones, where m are positive integers. Nevertheless, with the increase of molecular size, these oscillations are progressively reduced, and eventually absent for sufficiently large n. Accordingly, the S_{vN} values of c-CC[n] are oscillatory only for smaller n (up to n = 73), and become monotonically increasing for larger n. Since the S_{vN} value can be regarded as a quantitative measure of the radical nature of a molecule, the larger l-CC[n]/c-CC[n] are expected to exhibit increasing polyradical nature in their ground states.

Active orbital occupation numbers. To understand the reason that the symmetrized von Neumann entropy grows with the size of l-CC[n]/c-CC[n], it is instructive and informative to present the active orbital occupation numbers of ground-state l-CC[n]/c-CC[n] (consisting of N electrons), obtained with spin-restricted TAO-LDA, wherein the highest occupied molecular orbital (HOMO) is defined as the $(N/2)$th orbital, the lowest unoccupied molecular orbital (LUMO) is defined as the $(N/2 + 1)$th orbital, and so forth[49,51,58,60–62]. Here, the active orbitals are regarded as the orbitals with an occupation number ranging from 0.2 to 1.8 (i.e., the active spin-orbitals are regarded as the spin-orbitals with an occupation number ranging from 0.1 to 0.9).

As shown in Fig. 5, the active orbital occupation numbers of the smaller l-CC[n] (e.g., up to n = 20) reveal odd-even oscillation patterns, indicating that odd-numbered l-CC[n] possess nonradical nature (i.e., the occupation numbers of all orbitals are close to either 0 or 2), and even-numbered l-CC[n] possess pronounced diradical nature (i.e., the active orbitals are HOMO and LUMO). However, with the increase of the size of l-CC[n], the active orbital occupation numbers become closer to 1 and/or the number of active orbitals increases, suggesting an increasing polyradical nature of the larger l-CC[n].

In contrast to l-CC[n], the active orbital occupation numbers of c-CC[n] display very different patterns (see Fig. 6). In particular, the smaller c-CC[$4m + 2$] (e.g., up to $4m + 2$ = 46) possess nonradical nature (i.e., the occupation numbers of all orbitals are close to either 0 or 2), and hence are relatively more stable than c-CC[$4m$], c-CC[$4m + 1$], and c-CC[$4m + 3$], where m are positive integers. By contrast, c-CC[$4m$] (where m are positive integers) possess tetraradical nature (i.e., the active orbitals are HOMO−1, HOMO, LUMO, and LUMO+1). Nevertheless, with the increase of the size of c-CC[n], the active orbital occupation numbers become closer to 1 and/or the number of active orbitals increases, suggesting an increasing polyradical nature of the larger c-CC[n].

On the basis of the active orbital occupation numbers, the smaller odd-numbered l-CC[n] and the smaller c-CC[$4m + 2$] (where m are positive integers) possess nonradical nature in their ground states, being consistent with the analyses of the other electronic properties (e.g., the larger E_{ST} values, larger E_{SQ} values, larger E_g values, and smaller S_{vN} values) of these relatively stable linear carbon chains and cyclic carbon chains, respectively. Accordingly, this study confirms the high stability of the smaller c-CC[$4m + 2$][24,25], including the recently synthesized c-CC[18][26]. On the other hand, c-CC[$4m$] (where m are positive integers) possess tetraradical nature in their ground states, also showing consistency with the analyses of the other electronic properties (e.g., the

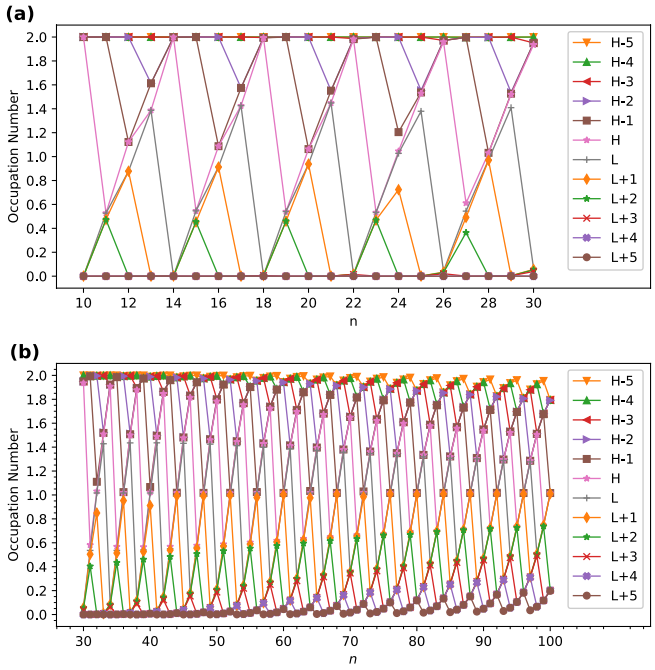

Figure 6. Active orbital occupation numbers (HOMO−5,...,HOMO−1, HOMO, LUMO, LUMO+1,...,and LUMO+5) of ground-state *c*-CC[*n*] with (**a**) $n = 10–30$ and (**b**) $n = 30–100$, calculated using spin-restricted TAO-LDA. For brevity, HOMO/LUMO is denoted as H/L.

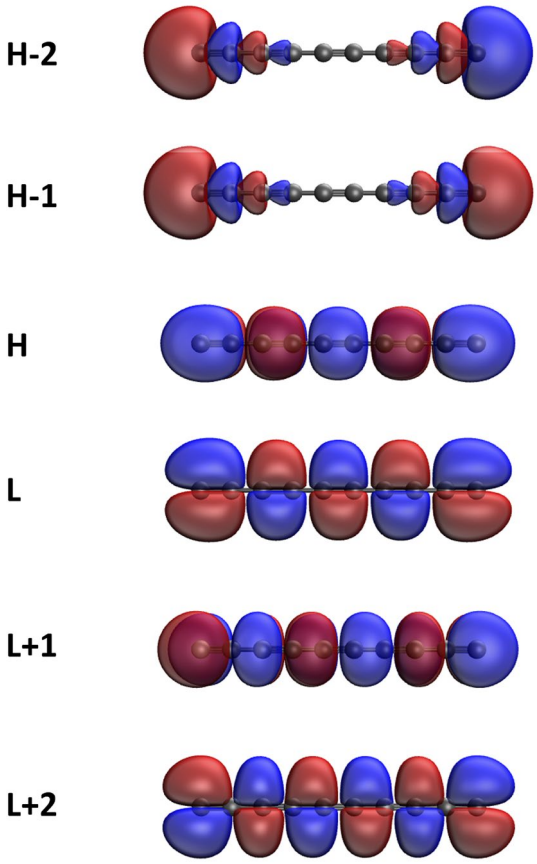

Figure 7. Real-space representation of HOMO−2 (1.952), HOMO−1 (1.951), HOMO (1.049), LUMO (1.049), LUMO+1 (0.000), and LUMO+2 (0.000) of ground-state *l*-CC[10], calculated using spin-restricted TAO-LDA, at isovalue = 0.02 e/Å^3. The orbital occupation numbers are given in parentheses. For brevity, HOMO/LUMO is denoted as H/L.

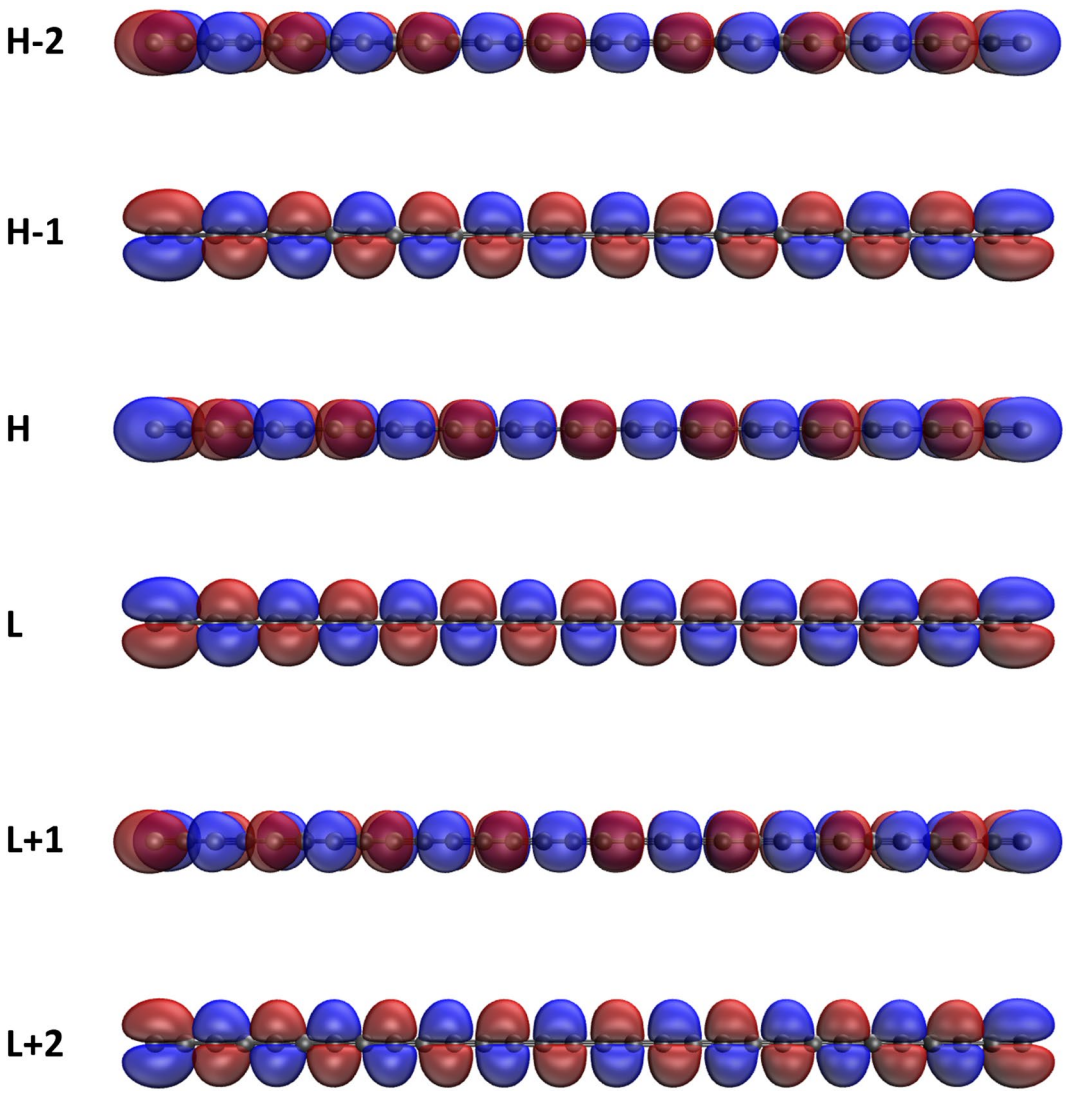

Figure 8. Real-space representation of HOMO−2 (1.914), HOMO−1 (1.914), HOMO (1.063), LUMO (1.063), LUMO+1 (0.064), and LUMO+2 (0.064) of ground-state *l*-CC[30], calculated using spin-restricted TAO-LDA, at isovalue = 0.02 e/Å^3. The orbital occupation numbers are given in parentheses. For brevity, HOMO/LUMO is denoted as H/L.

smaller E_{ST} values, smaller E_{SQ} values, smaller E_g values, and larger S_{vN} values) of these relatively unstable cyclic carbon chains.

Real-space representation of active orbitals. Here, we plot the real-space representation of the active orbitals, such as HOMO−2, HOMO−1, HOMO, LUMO, LUMO+1, and LUMO+2, for the ground states of some representative *l*-CC[*n*] (see Figs. 7 and 8) and *c*-CC[*n*] (see Figs. 9 and 10), obtained with spin-restricted TAO-LDA (also see Figures S1 to S6 in SI for more illustrative cases). The real-space representation analysis indicates that the active orbitals are delocalized over the entire length of *l*-CC[*n*] or the whole circumference of *c*-CC[*n*]. As the electrical conductivities of molecules consisting of many delocalized electrons are likely to be high[70], it can be anticipated that *l*-CC[*n*]/*c*-CC[*n*] should be highly conductive due to the presence of delocalized electrons.

Relative stability. We carry out spin-unrestricted TAO-LDA calculations to investigate the relative stability of *l*-CC[*n*] and *c*-CC[*n*] (i.e., the two isomers) in their ground states, which is examined by

$$E_{rel} = E_S(l\text{-}CC) - E_S(c\text{-}CC). \quad (7)$$

Here, E_{rel} is the relative energy of ground-state *l*-CC[*n*] with respect to ground-state *c*-CC[*n*], and $E_S(l\text{-}CC)$ and $E_S(c\text{-}CC)$ are the lowest singlet state (i.e., ground state) energies of *l*-CC[*n*] and *c*-CC[*n*], respectively.

The E_{rel} value as a function of the number of carbon atoms is plotted in Fig. 11 (also see Table S5 in SI). As the system size increases, the E_{rel} values are oscillatory only for smaller values of n (up to $n = 59$), and become

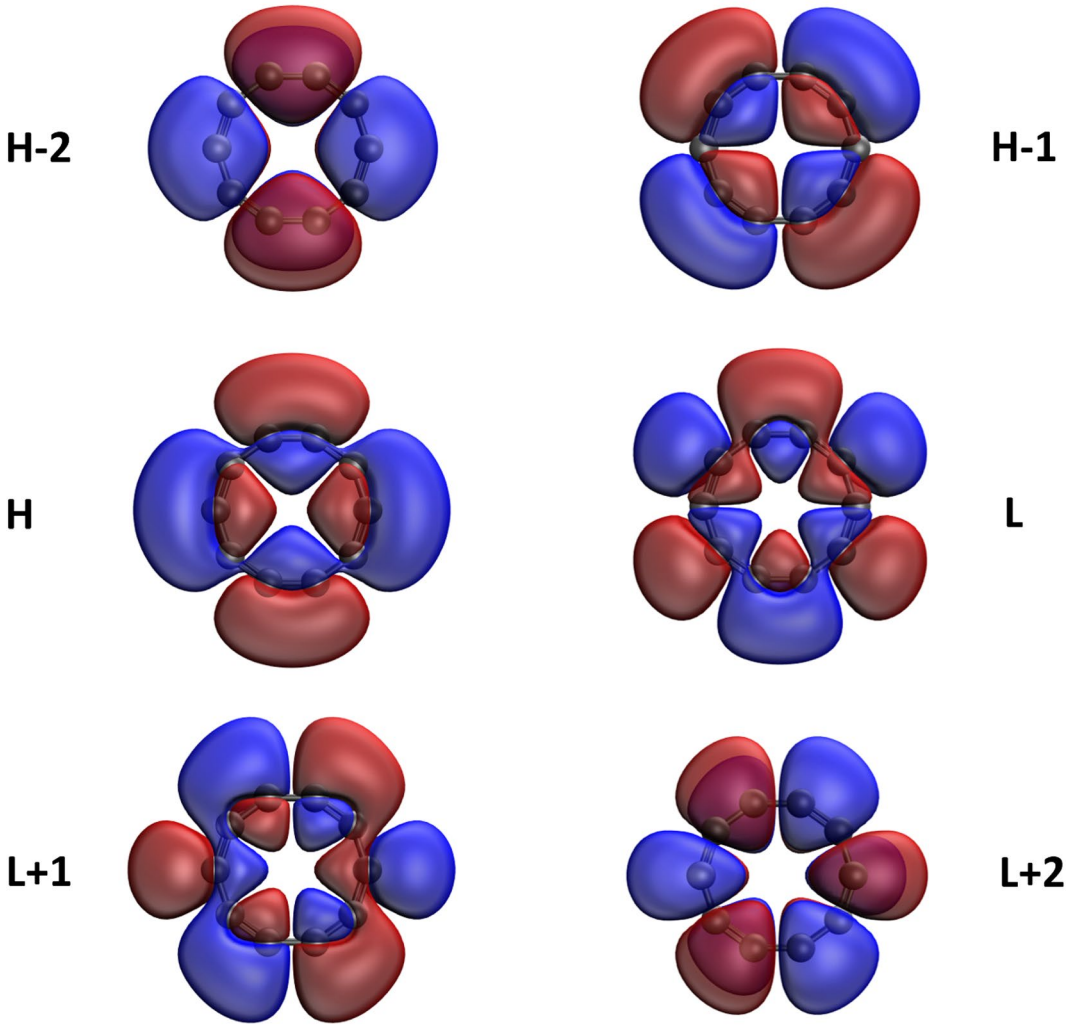

Figure 9. Real-space representation of HOMO−2 (2.000), HOMO−1 (2.000), HOMO (2.000), LUMO (0.000), LUMO+1 (0.000), and LUMO+2 (0.000) of ground-state *c*-CC[10], calculated using spin-restricted TAO-LDA, at isovalue = 0.02 e/Å^3. The orbital occupation numbers are given in parentheses. For brevity, HOMO/LUMO is denoted as H/L.

monotonically increasing for larger n. For all the cases investigated, *c*-CC[n] are energetically more stable than *l*-CC[n], showing the significance of cyclic topology.

Conclusions

In conclusion, we have employed TAO-DFT to investigate the electronic properties (e.g., the singlet-triplet energy gap, singlet-quintet energy gap, vertical ionization potential, vertical electron affinity, fundamental gap, symmetrized von Neumann entropy, active orbital occupation numbers, real-space representation of active orbitals, and relative stability) of *l*-CC[n]/*c*-CC[n] with n = 10–100 carbon atoms. For considerably large n, *l*-CC[n]/*c*-CC[n] are polyradicals in their ground states, playing an important role in determining their electronic properties. In view of their polyradical nature, it can be unreliable to study the properties of the larger *l*-CC[n]/*c*-CC[n] using KS-DFT with the traditional XC energy functionals, and it can be computationally intractable to study the properties of the larger *l*-CC[n]/*c*-CC[n] using accurate MR electronic structure methods. Consequently, it is well justified to study the electronic properties of *l*-CC[n]/*c*-CC[n] using TAO-DFT (i.e., a computationally efficient electronic structure method for nanosystems with radical nature) in this work.

For all the cases investigated, *l*-CC[n] and *c*-CC[n] are ground-state singlets, and *c*-CC[n] are energetically more stable than *l*-CC[n]. The electronic properties of *l*-CC[n] and *c*-CC[n] display peculiar oscillation patterns for smaller values of n, followed by monotonic changes for larger values of n. For the smaller carbon chains, odd-numbered *l*-CC[n] are more stable than the adjacent even-numbered ones, and *c*-CC[$4m + 2$]/*c*-CC[$4m$] (where m are positive integers) are more/less stable than the adjacent odd-numbered ones. With the increase of n, *l*-CC[n] and *c*-CC[n] possess increasing polyradical nature in their ground states, with the active orbitals being delocalized over the entire length of *l*-CC[n] or the whole circumference of *c*-CC[n].

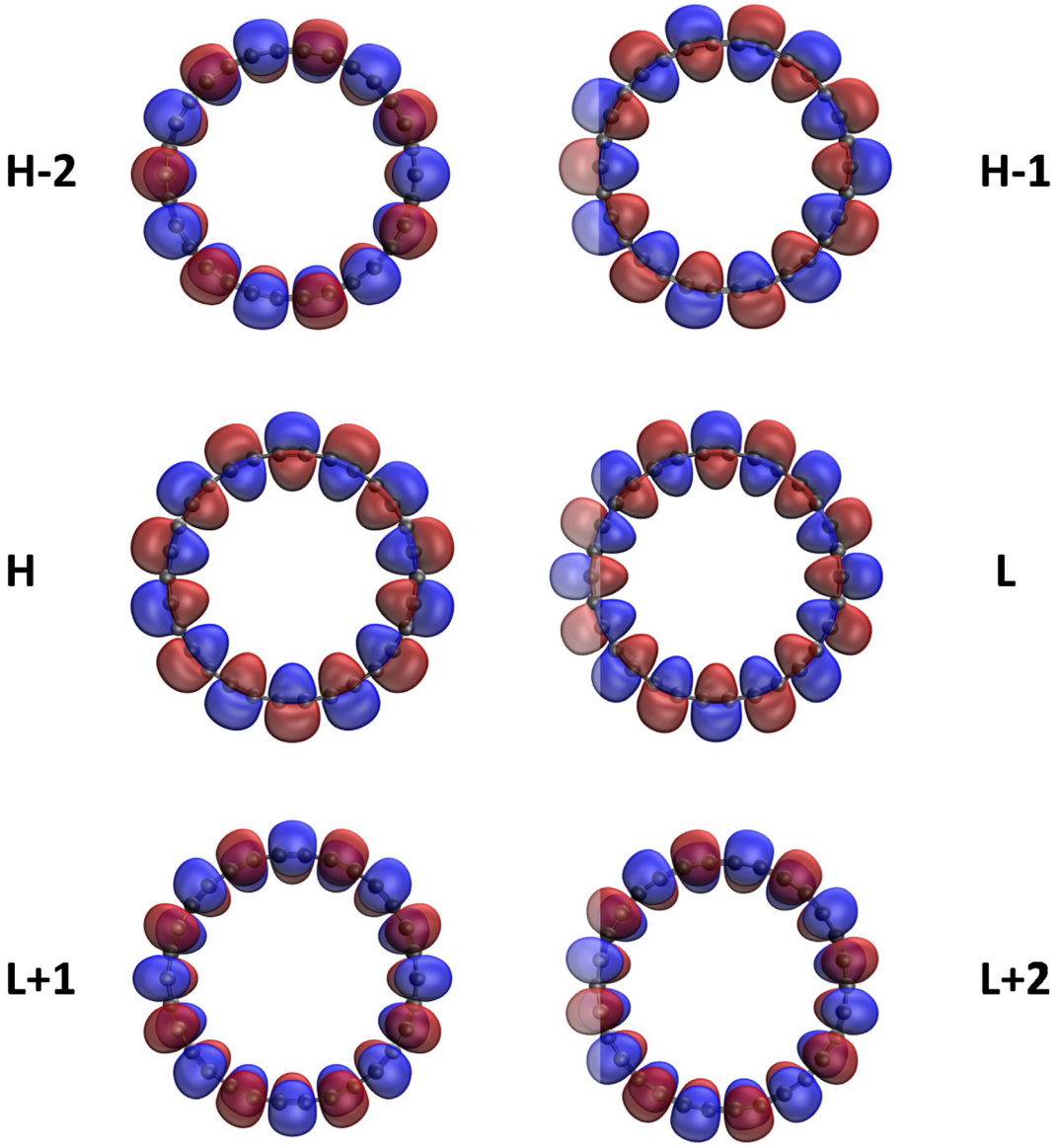

Figure 10. Real-space representation of HOMO−2 (1.950), HOMO−1 (1.949), HOMO (1.935), LUMO (0.066), LUMO+1 (0.057), and LUMO+2 (0.053) of ground-state *c*-CC[30], calculated using spin-restricted TAO-LDA, at isovalue = 0.02 e/Å^3. The orbital occupation numbers are given in parentheses. For brevity, HOMO/LUMO is denoted as H/L.

On the basis of our TAO-LDA results, the smaller *c*-CC[$4m + 2$] (up to $4m + 2 = 22$, where m are positive integers) possess nonradical nature and sizable singlet-triplet energy gaps (e.g., larger than 20 kcal/mol). In view of their high stability, it can be anticipated that these relatively stable cyclic carbon chains, such as *c*-CC[10], *c*-CC[14], *c*-CC[18], and *c*-CC[22], are likely to be synthesized in the near future. Note that among them, *c*-CC[18] have been recently synthesized[26].

While the method adopted (i.e., TAO-LDA with the fictitious temperature $\theta = 7$ mhartree[49]) is computationally efficient for the study of nanosystems with radical nature, a few limitations remain. First, owing to the use of LDA XC and θ-dependent density functionals in TAO-DFT, TAO-LDA can yield the self-interaction error[41,49,51], and hence bond length alternation (BLA) can be suppressed[30]. Second, the present θ value is system-independent, and hence the static correlation associated with electronic systems can only be described approximately[53]. Note that the first issue can be greatly resolved by using the long-range corrected hybrid XC functionals[71,72] in TAO-DFT[51,52] for an improved description of nonlocal exchange effects, and the second issue can be greatly resolved by using the respective self-consistent scheme for determining the θ value[53]. Accordingly, we plan to work in this direction in the future.

On the other hand, to fully understand the impact of molecular geometries (e.g., BLA) on the electronic properties (e.g., the singlet-triplet energy gap, singlet-quintet energy gap, fundamental gap, and active orbital occupation numbers) of *l*-CC[*n*]/*c*-CC[*n*], it is essential to employ accurate multi-reference methods, such as

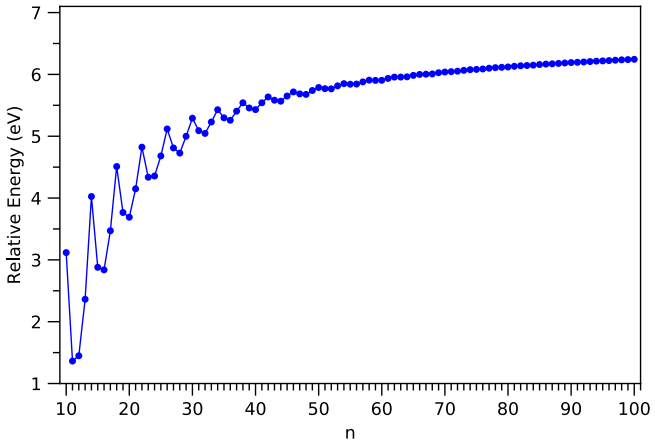

Figure 11. Relative energy of ground-state *l*-CC[*n*] with respect to ground-state *c*-CC[*n*] for *n* = 10–100, calculated using spin-unrestricted TAO-LDA.

the CASSCF (for static correlation) and possibly, CASPT2 (for both static correlation and dynamical correlation) methods, for geometry optimizations and single-point energy calculations on different spin states (e.g., the lowest singlet, triplet, and quintet states) of *l*-CC[*n*]/*c*-CC[*n*]. As this task can be computationally intractable, the electronic properties of *l*-CC[*n*]/*c*-CC[*n*] calculated using reasonably accurate and relatively inexpensive multi-reference methods are needed.

Data availability

The data that support the findings of this study are available from the corresponding author upon reasonable request.

Received: 22 April 2020; Accepted: 22 July 2020
Published online: 04 August 2020

References

1. Kroto, H. W., Heath, J. R., O'Brien, S. C., Curl, R. F. & Smalley, R. E. C_{60}: Buckminsterfullerene. *Nature* **318**, 162–163 (1985).
2. Novoselov, K. S. *et al.* Electric field effect in atomically thin carbon films. *Science* **306**, 666–669 (2004).
3. Georgakilas, V., Perman, J. A., Tucek, J. & Zboril, R. Broad family of carbon nanoallotropes: Classification, chemistry, and applications of fullerenes, carbon dots, nanotubes, graphene, nanodiamonds, and combined superstructures. *Chem. Rev.* **115**, 4744–4822 (2015).
4. Iijima, S. Helical microtubules of graphitic carbon. *Nature* **354**, 56–58 (1991).
5. Baeyer, A. Ueber polyacetylenverbindungen. *Ber. Dtsch. Chem. Ges.* **18**, 2269–2281 (1885).
6. Zhao, X., Ando, Y., Liu, Y., Jinno, M. & Suzuki, T. Carbon nanowire made of a long linear carbon chain inserted inside a multiwalled carbon nanotube. *Phys. Rev. Lett.* **90**, 187401 (2003).
7. Belau, L. *et al.* Ionization thresholds of small carbon clusters: Tunable VUV experiments and theory. *J. Am. Chem. Soc.* **129**, 10229–10243 (2007).
8. Jin, C., Lan, H., Peng, L., Suenaga, K. & Iijima, S. Deriving carbon atomic chains from graphene. *Phys. Rev. Lett.* **102**, 205501 (2009).
9. Liu, M., Artyukhov, V. I., Lee, H., Xu, F. & Yakobson, B. I. Carbyne from first principles: Chain of C atoms, a nanorod or a nanorope. *ACS Nano* **7**, 10075–10082 (2013).
10. Artyukhov, V. I., Liu, M. & Yakobson, B. I. Mechanically induced metal-insulator transition in carbyne. *Nano Lett.* **14**, 4224–4229 (2014).
11. Andrade, N. F. *et al.* Linear carbon chains under high-pressure conditions. *J. Phys. Chem. C* **119**, 10669–10676 (2015).
12. Banhart, F. Chains of carbon atoms: A vision or a new nanomaterial?. *Beilstein J. Nanotechnol.* **6**, 559–569 (2015).
13. Casari, C. S., Tommasini, M., Tykwinski, R. R. & Milani, A. Carbon-atom wires: 1-D systems with tunable properties. *Nanoscale* **8**, 4414–4435 (2016).
14. Shi, L. *et al.* Confined linear carbon chains as a route to bulk carbyne. *Nat. Mater.* **15**, 634–639 (2016).
15. Shi, L. *et al.* Electronic band gaps of confined linear carbon chains ranging from polyyne to carbyne. *Phys. Rev. Mater.* **1**, 075601 (2017).
16. Seenithurai, S. & Chai, J.-D. Effect of Li termination on the electronic and hydrogen storage properties of linear carbon chains: A TAO-DFT study. *Sci. Rep.* **7**, 4966 (2017).
17. Casari, C. S. & Milani, A. Carbyne: From the elusive allotrope to stable carbon atom wires. *MRS Commun.* **8**, 207–219 (2018).
18. Heeg, S., Shi, L., Poulikakos, L. V., Pichler, T. & Novotny, L. Carbon nanotube chirality determines properties of encapsulated linear carbon chain. *Nano Lett.* **18**, 5426–5431 (2018).
19. Hoffmann, R. Extended Hückel theory-V: Cumulenes, polyenes, polyacetylenes and C_n. *Tetrahedron* **22**, 521–538 (1966).
20. Yang, S. *et al.* UPS of 2–30-atom carbon clusters: Chains and rings. *Chem. Phys. Lett.* **144**, 431–436 (1988).
21. von Helden, G., Gotts, N. G. & Bowers, M. T. Experimental evidence for the formation of fullerenes by collisional heating of carbon rings in the gas phase. *Nature* **363**, 60–63 (1993).
22. Handschuh, H., Ganteför, G., Kessler, B., Bechthold, P. S. & Eberhardt, W. Stable configurations of carbon clusters: Chains, rings, and fullerenes. *Phys. Rev. Lett.* **74**, 1095–1098 (1995).
23. Kaizu, K. *et al.* Neutral carbon cluster distribution upon laser vaporization. *J. Chem. Phys.* **106**, 9954 (1997).
24. Van Orden, A. & Saykally, R. J. Small carbon clusters: Spectroscopy, structure, and energetics. *Chem. Rev.* **98**, 2313–2358 (1998).

25. Wakabayashi, T., Momose, T. & Shida, T. Mass spectroscopic studies of laser ablated carbon clusters as studied by photoionization with 10.5 eV photons under high vacuum. *J. Chem. Phys.* **111**, 6260–6263 (1999).
26. Kaiser, K. *et al.* An *sp*-hybridized molecular carbon allotrope, cyclo[18]carbon. *Science* **365**, 1299–1301 (2019).
27. Lu, T., Chen, Q. & Liu, Z. A thorough theoretical exploration of intriguing characteristics of cyclo[18]carbon: Geometry, bonding nature, aromaticity, weak interaction, reactivity, excited states, vibrations, molecular dynamics and various molecular properties. *ChemRxiv*, Preprint. https://doi.org/10.26434/chemrxiv.11320130.v2 (2019).
28. Stasyuk, A. J., Stasyuk, O. A., Solà, M. & Voityuk, A. A. Cyclo[18]carbon: The smallest all-carbon electron acceptor. *Chem. Commun.* **56**, 352–355 (2020).
29. Martin, J. M. L., El-Yazal, J. & François, J.-P. Structure and vibrational spectra of carbon clusters C_n (n = 2–10, 12, 14, 16, 18) using density functional theory including exact exchange contributions. *Chem. Phys. Lett.* **242**, 570–579 (1995).
30. Heaton-Burgess, T. & Yang, W. Structural manifestation of the delocalization error of density functional approximations: C_{4N+2} rings and C_{20} bowl, cage, and ring isomers. *J. Chem. Phys.* **132**, 234113 (2010).
31. Shi, B., Yuan, L., Tang, T., Yuan, Y. & Tang, Y. Study on electronic structure and excitation characteristics of cyclo[18]carbon. *Chem. Phys. Lett.* **741**, 136975 (2020).
32. Pereira, Z. S. & da Silva, E. Z. Spontaneous symmetry breaking in cyclo[18]carbon. *J. Phys. Chem. A* **124**, 1152–1157 (2020).
33. Li, M. *et al.* Potential molecular semiconductor devices: Cyclo-C_n (n = 10 and 14) with higher stabilities and aromaticities than acknowledged cyclo-C_{18}. *Phys. Chem. Chem. Phys.* **22**, 4823–4831 (2020).
34. Hong, I. *et al.* Competition between Hückel's rule and Jahn-Teller distortion in small carbon rings: A quantum Monte Carlo study. *J. Phys. Chem. A* **124**, 3636–3640 (2020).
35. Brémond, É, Pérez-Jiménez, ÁJ., Adamo, C. & Sancho-García, J. C. sp-hybridized carbon allotrope molecular structures: An ongoing challenge for density-functional approximations. *J. Chem. Phys.* **151**, 211104 (2019).
36. Zou, W., Tao, Y. & Kraka, E. Systematic description of molecular deformations with Cremer-Pople puckering and deformation coordinates utilizing analytic derivatives: Applied to cycloheptane, cyclooctane, and cyclo[18]carbon. *J. Chem. Phys.* **152**, 154107 (2020).
37. Baryshnikov, G. V., Valiev, R. R., Kuklin, A. V., Sundholm, D. & Ågren, H. Cyclo[18]carbon: Insight into electronic structure, aromaticity, and surface coupling. *J. Phys. Chem. Lett.* **10**, 6701–6705 (2019).
38. Zhang, L., Li, H., Feng, Y. P. & Shen, L. Diverse transport behaviors in cyclo[18]carbon-based molecular devices. *J. Phys. Chem. Lett.* **11**, 2611–2617 (2020).
39. Brus, L. Size, dimensionality, and strong electron correlation in nanoscience. *Acc. Chem. Res.* **47**, 2951–2959 (2014).
40. Kohn, W. & Sham, L. J. Self-consistent equations including exchange and correlation effects. *Phys. Rev.* **140**, A1133–A1138 (1965).
41. Cohen, A. J., Mori-Sánchez, P. & Yang, W. Challenges for density functional theory. *Chem. Rev.* **112**, 289–320 (2012).
42. Andersson, K., Malmqvist, P. -Å & Roos, B. O. Second-order perturbation theory with a complete active space self-consistent field reference function. *J. Chem. Phys.* **96**, 1218–1226 (1992).
43. Hachmann, J., Dorando, J. J., Aviles, M. & Chan, G. K. L. The radical character of the acenes: A density matrix renormalization group study. *J. Chem. Phys.* **127**, 134309 (2007).
44. Gidofalvi, G. & Mazziotti, D. A. Active-space two-electron reduced-density-matrix method: Complete active-space calculations without diagonalization of the N-electron hamiltonian. *J. Chem. Phys.* **129**, 134108 (2008).
45. Gryn'ova, G., Coote, M. L. & Corminboeuf, C. Theory and practice of uncommon molecular electronic configurations. *WIREs Comput. Mol. Sci.* **5**, 440–459 (2015).
46. Fosso-Tande, J., Nguyen, T.-S., Gidofalvi, G. & DePrince, A. E. III. Large-scale variational two-electron reduced-density-matrix-driven complete active space self-consistent field methods. *J. Chem. Theory Comput.* **12**, 2260–2271 (2016).
47. Battaglia, S., Faginas-Lago, N., Andrae, D., Evangelisti, S. & Leininger, T. Increasing radical character of large [n]cyclacenes unveiled by wave function theory. *J. Phys. Chem. A* **121**, 3746–3756 (2017).
48. Mullinax, J. W. *et al.* Heterogeneous CPU + GPU algorithm for variational two-electron reduced-density matrix-driven complete active-space self-consistent field theory. *J. Chem. Theory Comput.* **15**, 6164–6178 (2019).
49. Chai, J.-D. Density functional theory with fractional orbital occupations. *J. Chem. Phys.* **136**, 154104 (2012).
50. Chai, J.-D. Thermally-assisted-occupation density functional theory with generalized-gradient approximations. *J. Chem. Phys.* **140**, 18A521 (2014).
51. Chai, J.-D. Role of exact exchange in thermally-assisted-occupation density functional theory: A proposal of new hybrid schemes. *J. Chem. Phys.* **146**, 044102 (2017).
52. Xuan, F., Chai, J.-D. & Su, H. Local density approximation for the short-range exchange free energy functional. *ACS Omega* **4**, 7675–7683 (2019).
53. Lin, C.-Y., Hui, K., Chung, J.-H. & Chai, J.-D. Self-consistent determination of the fictitious temperature in thermally-assisted-occupation density functional theory. *RSC Adv.* **7**, 50496–50507 (2017).
54. Wu, C.-S. & Chai, J.-D. Electronic properties of zigzag graphene nanoribbons studied by TAO-DFT. *J. Chem. Theory Comput.* **11**, 2003–2011 (2015).
55. Yeh, C.-N. & Chai, J.-D. Role of Kekulé and non-Kekulé structures in the radical character of alternant polycyclic aromatic hydrocarbons: A TAO-DFT study. *Sci. Rep.* **6**, 30562 (2016).
56. Seenithurai, S. & Chai, J.-D. Effect of Li adsorption on the electronic and hydrogen storage properties of acenes: A dispersion-corrected TAO-DFT study. *Sci. Rep.* **6**, 33081 (2016).
57. Wu, C.-S., Lee, P.-Y. & Chai, J.-D. Electronic properties of cyclacenes from TAO-DFT. *Sci. Rep.* **6**, 37249 (2016).
58. Yeh, C.-N., Wu, C., Su, H. & Chai, J.-D. Electronic properties of the coronene series from thermally-assisted-occupation density functional theory. *RSC Adv.* **8**, 34350–34358 (2018).
59. Seenithurai, S. & Chai, J.-D. Electronic and hydrogen storage properties of Li-terminated linear boron chains studied by TAO-DFT. *Sci. Rep.* **8**, 13538 (2018).
60. Chung, J.-H. & Chai, J.-D. Electronic properties of Möbius cyclacenes studied by thermally-assisted-occupation density functional theory. *Sci. Rep.* **9**, 2907 (2019).
61. Seenithurai, S. & Chai, J.-D. Electronic properties of linear and cyclic boron nanoribbons from thermally-assisted-occupation density functional theory. *Sci. Rep.* **9**, 12139 (2019).
62. Deng, Q. & Chai, J.-D. Electronic properties of triangle-shaped graphene nanoflakes from TAO-DFT. *ACS Omega* **4**, 14202–14210 (2019).
63. Hanson-Heine, M. W. D. Static correlation in vibrational frequencies studied using thermally-assisted-occupation density functional theory. *Chem. Phys. Lett.* **739**, 137012 (2020).
64. Pérez-Guardiola, A. *et al.* The role of topology in organic molecules: Origin and comparison of the radical character in linear and cyclic oligoacenes and related oligomers. *Phys. Chem. Chem. Phys.* **20**, 7112–7124 (2018).
65. Pérez-Guardiola, A. *et al.* From cyclic nanorings to single-walled carbon nanotubes: Disclosing the evolution of their electronic structure with the help of theoretical methods. *Phys. Chem. Chem. Phys.* **21**, 2547–2557 (2019).
66. Yoshikawa, T., Doi, T. & Nakai, H. Finite-temperature-based linear-scaling divide-and-conquer self-consistent field method for static electron correlation systems. *Chem. Phys. Lett.* **725**, 18–23 (2019).
67. Shao, Y. *et al.* Advances in molecular quantum chemistry contained in the Q-Chem 4 program package. *Mol. Phys.* **113**, 184–215 (2015).

68. Smith, M. B. & Michl, J. Singlet fission. *Chem. Rev.* **110**, 6891–6936 (2010).
69. Rivero, P., Jiménez-Hoyos, C. A. & Scuseria, G. E. Entanglement and polyradical character of polycyclic aromatic hydrocarbons predicted by projected Hartree-Fock theory. *J. Phys. Chem. B* **117**, 12750–12758 (2013).
70. Che, Y. *et al.* Enhancing one-dimensional charge transport through intermolecular π-electron delocalization: Conductivity improvement for organic nanobelts. *J. Am. Chem. Soc.* **129**, 6354–6355 (2007).
71. Cohen, A. J., Mori-Sánchez, P. & Yang, W. Development of exchange-correlation functionals with minimal many-electron self-interaction error. *J. Chem. Phys.* **126**, 191109 (2007).
72. Lin, Y.-S., Li, G.-D., Mao, S.-P. & Chai, J.-D. Long-range corrected hybrid density functionals with improved dispersion corrections. *J. Chem. Theory Comput.* **9**, 263–272 (2013).

Acknowledgements

This work was supported by the Ministry of Science and Technology of Taiwan (Grant No. MOST107-2628-M-002-005-MY3), National Taiwan University (Grant No. NTU-CDP-105R7818), and the National Center for Theoretical Sciences of Taiwan.

Author contributions

S.S. and J.-D.C. designed the project, performed the data analysis, and wrote the manuscript. S.S. carried out the calculations.

Competing interests

The authors declare no competing interests.

Additional information

Supplementary information is available for this paper at https://doi.org/10.1038/s41598-020-70023-z.

Correspondence and requests for materials should be addressed to J.-D.C.

Reprints and permissions information is available at www.nature.com/reprints.

Publisher's note Springer Nature remains neutral with regard to jurisdictional claims in published maps and institutional affiliations.